Scientific Research Publishing

Open Journal of Microphysics, 2024, 14, 1-12
https://www.scirp.org/journal/ojm
ISSN Online: 2162-2469
ISSN Print: 2162-2450

Density Functional Calculations of the Mechanical, Electronic and Dynamical Properties of Antiperovskite Ca_3BO (B = Pb, Ge, Sn)

Phillip Wilfsen Otieno Nyawere

Department of Physical and Biological Sciences, Kabarak University, Nakuru, Kenya
Email: pnyawere@gmail.com

How to cite this paper: Nyawere, P.W.O. (2024) Density Functional Calculations of the Mechanical, Electronic and Dynamical Properties of Antiperovskite Ca_3BO (B = Pb, Ge, Sn). *Open Journal of Microphysics*, **14**, 1-12.
https://doi.org/10.4236/ojm.2024.141001

Received: April 14, 2023
Accepted: February 26, 2024
Published: February 29, 2024

Abstract

An analysis of mechanical, electronic and dynamical properties of antiperovskite Ca_3BO (B = Pb, Ge, Sn) in cubic phase space group Pm-3m (221) has been studied using first principle density functional theory (DFT). Ground state energy computation was done using the Projector Augmented Wave (PAW) Pseudo Potentials and the Plane Wave (PW) basis set. The Generalized Gradient Approximation (GGA) was used for the exchange correlation. The open source code QUANTUM ESPRESSO (QE) was used in this study in which plane wave basis sets are applied for the expansion of the electronic structure wave function. Thermo_pw as a post-processing code was used for the computation of mechanical properties including bulk modulus and elastic constants with their derivatives. The lattice parameters are here calculated to be 4.87 Å, 4.86 Å and 4.84 Å for Ca_3BO (B = Pb, Ge, Sn) respectively which compares well with other works. This also shows that the three crystals are similar in size and in most of their properties. In addition to this, projected density of states and band structure are also computed both showing that these materials are of semi-metallic nature and are stable in cubic phase. Phonon modes at gamma are also reported.

Keywords

Antiperovskite, Elastic Constants, Generalized Gradient Approximation

1. Introduction

Inverse Perovskites or antiperovskite compounds have two types of anion and cation positions reversed. Their general formula is given as A_3BO where A sites

are occupied by an electropositive ion while B sites are occupied by different anions whose size is different from A. Antiperovskite has displayed interesting properties which include magnetism, ionic conductivity, superconductivity and thermoelectricity, [1] among others. The discovery of superconducting properties of cubic antiperovskite $MgCN_{i3}$ compound [2] has motivated research on more of these antiperovskites. These findings have prompted a new round of development of functional antiperovskites. A new class of antiperovskite compounds A_3BO where A = Ca, Sr, Ba and B = Pb have been reported to crystallize into the cubic inverse perovskite structure. Because of the varied properties of Antiperovskite materials, interests have shifted to their unusual high charge carrier mobility which leads to many technological applications [3]. There has been in the recent past growing research interest in band topology, leading to a broad classification of non-trivial topological metals classified as Weyl Semimetal, Dirac Semimetal and Nodal line Semimetal (NLS) [4]. These classified metals have their conduction band and valence hand crossing due to band inversion.

Three Dimensional (3D) Dirac fermion systems is a class of topological materials in which bulk conduction and valence bands with linear energy momentum dispersion relations meet at finite points or along curves in K-space. In order to verify the presence of 3D Dirac fermions theoretically, it is necessary to study electronic structure and in particular band structure to identify a Dirac point in 3D momentum space. The band structure of the inverse perovskite Ca_3PbO, through soft x-ray angle-resolved photoemission spectroscopy and cone like band dispersions are observed which is in close agreement with the predictions of electronic structure calculations [5].

The band structure calculation of Ca_3BO and its family using Wein2k have found that three-dimensional massive Dirac electrons exist at their Fermi energy. The present work is based on first principle calculations and demonstrates inverse perovskite phase of Ca_3BO (B = Pb, Sn, Ge) as the new candidates for realizing Dirac fermionic system. An investigation of structural, electronic and dynamical properties of Ca_3BO is reported using DFT-based simulation code Quantum Espresso (QE). The electronic band structure and the projected density of states (PDOS) have also been studied. The present computed results are found to be in good agreement with the already available experimental and theoretical results.

The rest of this paper is arranged such that Section II is Computational methodology, Section III is discussing results and Section IV are Conclusions.

2. Computational Methodology

Calculations in this work were done in the framework of density functional theory using for the exchange-correlation functional, the generalized gradient approximation method of Perdew-Burke Ernzerhof (PBE) [6]. The pseudopotentials were extracted from Quantum espresso database [7]. The total energy convergence in the iterative solution of the Kohn-Sham equations [8] was set at

2×10^{-8} Ry. Optimized cell dimensions were fitted in Murnaghan fitting methodology of second order. The k-points and the kinetic energy cut-off values were properly optimized to convergence at the ground state energy. The valence configuration used for Ca_3PbO was 4s and 3p for Ca, $6s^2$ for Pb and $2s^2$ for O. Similar criteria is used for the other two compounds where Pb is replaced with Ge and Sn. The Brillouin sampling was based on the Monkhost scheme [9] [10] [11]. The K-point mesh in the irreducible high symmetry points in the Brillouin zone used was $13 \times 13 \times 13$. For the elastic constant calculation, the "quasi-static" approximation was used where the elastic constants were computed at zero absolute temperature and saved as elastic constants.

3. Results

3.1. Structure Properties

Figure 1 shows the optimized unit cell of Ca_3PbO with Wyckoff positions given as Ca (0, 0.5, 0.5), Ca (0.5, 0, 0.5), Ca (0.5, 0.5, 0), O (0.5, 0.5, 0.5) and Pb (0, 0, 0). The structures of Ca_3SnO and Ca_3GeO are all similar to that of Ca_3PbO with the position of Pb, Sn and Ge being the same. The convergence was achieved at a pressure of zero GPa. The equilibrium lattice constants, bulk modulus and derived bulk modulus have been obtained by minimizing the total crystal energy. This minimum energy was calculated for different values of lattice constants using second order Birch-Murnaghan equation of states. The calculated values are represented in Table 1 for cubic phase of space group $Pm3\bar{m}$ (#221) for Ca_3BO (B = Pb, Ge, Sn). The lattice constants are 4.87Å, 4.86Å, and 4.84Å respectively for Ca_3BO (B = Pb, Ge, Sn) compounds which are found to compare well with other studies.

The three crystals show very close similarities in their sizes because of the similarity in the atoms in each crystal. The value of lattice parameters for all the three crystals are in agreement with other theoretical and experimental studies available. The values of bulk modulus and volume of single crystal also agrees

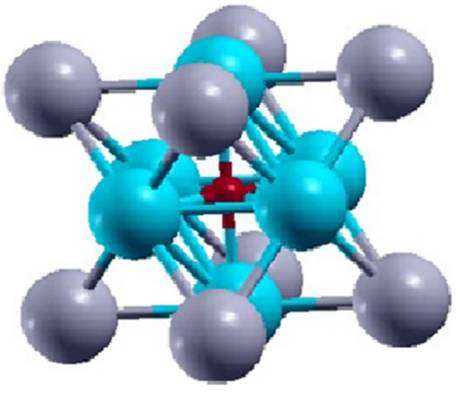

Figure 1. Optimized crystal structure of Ca_3PbO as visualized in xcrysden (Colour online) shows grey for O, light blue for Ca and red for Pb respectively. The central red at (0, 0, 0) is the position of Pb. It is this position that varies for Ca_3SnO and Ca_3GeO to be occupied by Sn and Ge respectively.

with the data of other studies.

Figure 2 shows the optimization of energy against lattice parameter. The lattice parameter was found to be 9.199 Bohr (4.87 Å) with volume of 115.35Å3 for Ca_3PbO. The optimization follows for all the three crystals.

3.2. Electronic Structure Properties

In this section, the partial density of states and band structures of Ca_3BO (B = Pb, Ge, Sn) are discussed. The Fermi energy for all these crystals was set at zero and they all show semi-metallic behaviour. In Figure 3, Ca_3PbO shows that above the Fermi level O-s states and Pb-s states are dominant even though other states also appear. Below the Femi level Ca-s-p states are more dominant. Ca_3GeO has Ge-s and Ca-s states in the conduction band and for Ca_3SnO there are Sn-s and Ca-s states. It is clearly seen that the electrons of metallic atoms are majorly responsible for the conduction of energy in the compounds. Ca_3PbO has

Table 1. Calculated lattice parameter (*a*), volume (*V*), bulk modulus (*B*) and pressure derivative of bulk modulus (d*B*/d*P*).

Material	*a* (Å)	*V* (Å^3)	*B* (GPa)	d*B*/d*P*
Ca_3PbO	4.87	115.35	51.79	4.33 (present)
	4.84 [12]	113.37	--	4.37 [14]
	4.73 [13]	105.82	64.59	
Ca3GeO	4.86	114.79	57.71	4.31 (present)
	4.73 [15]	105.7 [16]	57.71	
Ca_3SnO	4.84	113.38	55.08	3.67 (present)
	4.86 [17]	114.5 [17]		
	4.83 [18]	112.88		

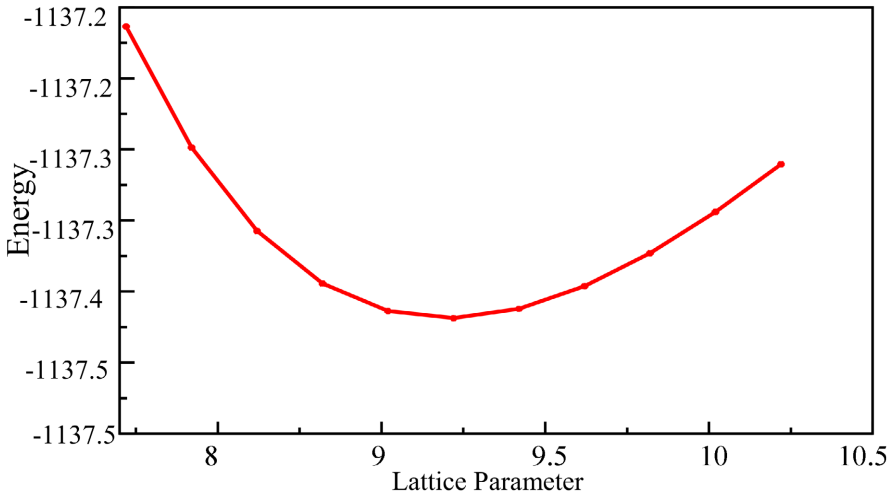

Figure 2. Optimized energy versus lattice parameter for Ca_3PbO. The minimum energy corresponding to the lattice parameter is shown. The behaviour of convergence is similar for all the other two crystals.

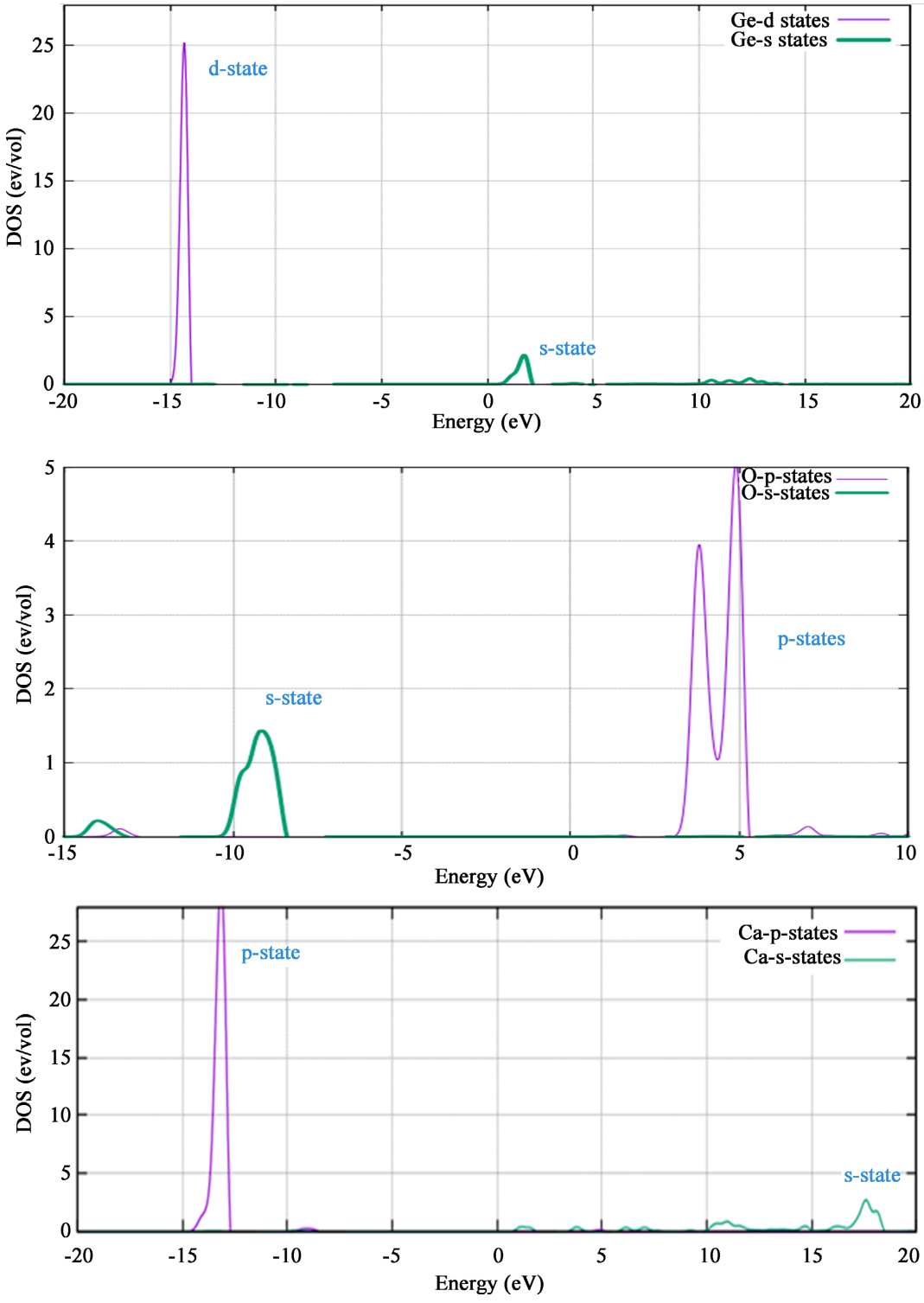

Figure 3. Projected density of states in electrons per electron-volt for the compound Ca_3BO. S-states, d-states and p-states are labelled.

more electrons on the conduction band making it better conductor compared to the rest. This could be attributed to the position of Pb in the periodic table that makes it contribute more valence electrons.

From Figure 3, it is seen that s-states of Ca and Ge are dominant in the conduction band but p-states are the ones dominant for Oxygen in the conduction band. This is expected to be the case for Ca_3SnO and Ca_3PbO compounds where oxygen is expected to behave in the similar way as in Ca_3GeO.

From Figure 4, the band structures are plotted and all the three compounds show semi-metallic nature with direct band gap for all the compounds. The high symmetry points are all similar with strikingly similar band structures. The only differences is the Fermi energy of each of the compounds for example for Fermi energy for Ca_3SnO is 8.64 eV and that of Ca_3PbO is 9.16 eV.

3.3. Mechanical Properties

The mechanical properties of Ca_3PbO were also simulated using thermo_pw code which is a post-processing code in quantum espresso to find the stability nature of this material. The cubic crystal has only three independent parameters which are C_{11}, C_{12} and C_{44}. For a solid under strain the elastic energy is given as [19],

$$\frac{\Delta E}{V} = \frac{1}{2}\sum_{i=1}^{6}\sum_{j=1}^{6} c_{ij} e_i e_j \tag{1}$$

where V is the undistorted lattice cell volume, ΔE is the change in energy from the strain vectors $e = (e, e_2, e_3, e_4, e_5, e_6)$ and c is the matrix of the elastic constants [20]. The Born's stability criteria [21] at zero pressure requires that the elastic constants are related such that: $C_{11} > 0$, $C_{11} - C_{12} > 0$, $C_{44} > 0$, $C_{11} + 2C_{12} > 0$ and $C_{11} > B > C_{12}$. These constants are calculated by using the obtained second-order elastic constants of Equation (2); the results are given in Table 2.

$$C_{ij} = \frac{1}{V_0}\frac{\partial^2 E_{tot}}{\partial \xi_i \partial \xi_j} \tag{2}$$

By using Born's stability rule, it can be seen that these compounds are stable. This is important in mechanical application where pressure is to be applied on the crystal like in thermoelectric energy generation [22].

The Zener anisotropy factor (A), Poisson ratio (δ), and Young's modulus (E) that are important parameters in understanding elastic properties are also calculated using these formulas [12];

$$A = \frac{2C_{44}}{C_{11} - C_{12}} \tag{3}$$

$$\delta = \frac{1}{2}\left\{\frac{B - \frac{2}{3}G}{B + \frac{1}{3}G}\right\} \tag{4}$$

$$E = \frac{9GB}{G + 3B} \tag{5}$$

where G is the isotropic shear modulus as a function of crystal orientation and is given as $G = (G_V + G_R)/2$, herein G_V is Voigt's shear modulus (which is related

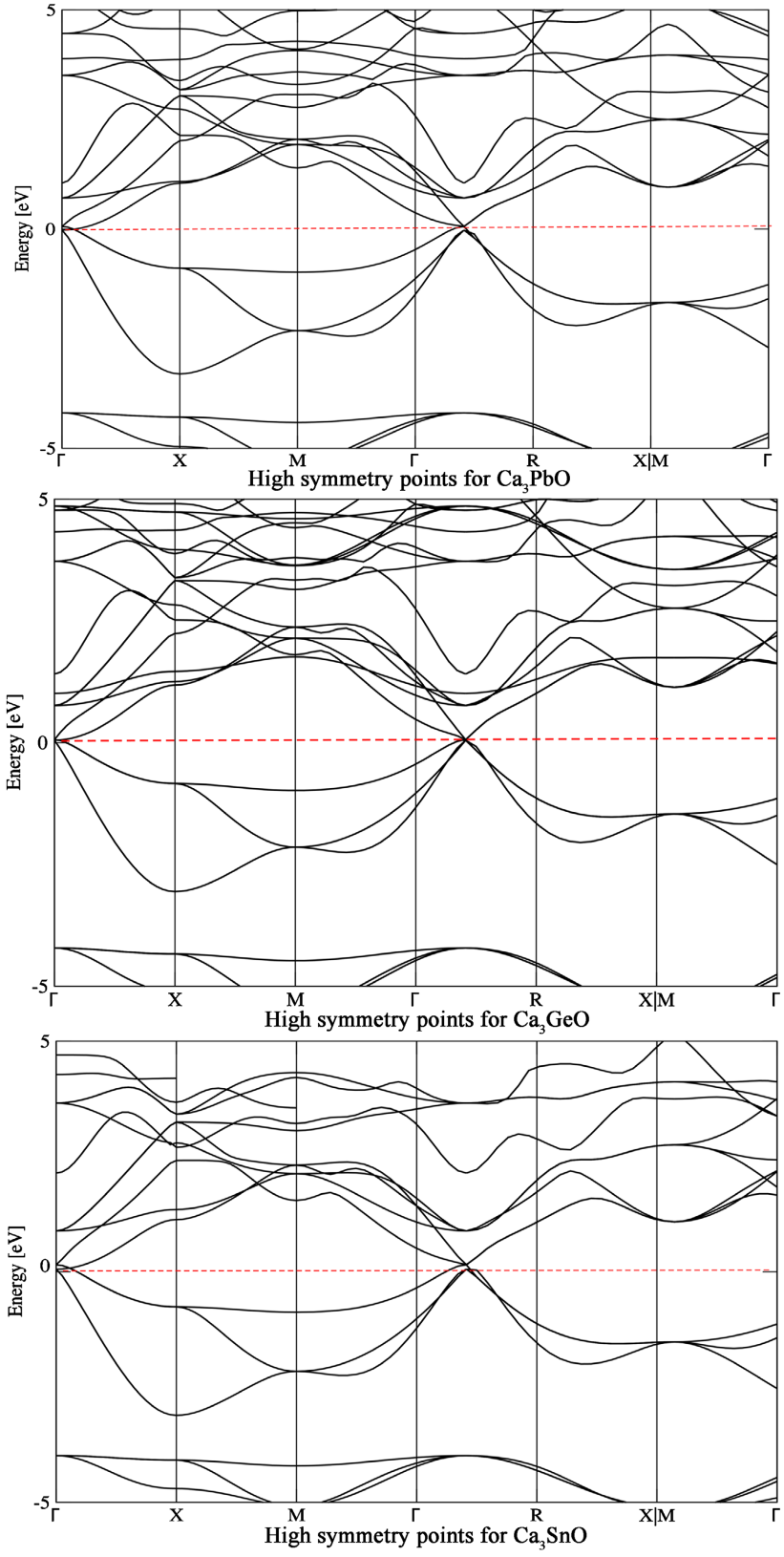

Figure 4. Bands of antiperovskite Ca_3PbO against the high symmetry points. The Fermi energy has been set at the origin. The diagram shows semi-metallic band behaviour. This behaviour is also depicted for the Ca_3SnO and Ca_3GeO crystals.

Table 2. Elastic constants, bulk modulus and stability.

Material	C_{11} (GPa)	C_{12} (GPa)	C_{44} (GPa)	B (GPa)	Stability
Ca_3PbO	97.68	28.71	49.09	51.7	Stable
Ca_3GeO	118.1	27.51	49.53	57.7	Stable
Ca_3SnO	103.32	30.96	50.49	55.08	Stable

Table 3. Voigt's shear modulus (G_V), Reuss's Shear modulus (G_R), Voigt's Young's modulus (E_V), Reuss Young's modulus (E_R), Poisson ratio (n), Zener anisotropy factor (A) and compressibility (β).

	Ca_3PbO	Ca_3SnO	Ca_3GeO
G_V (GPa)	41.98	44.77	47.83
G_R (GPa)	42.62	43.59	47.74
G/B	0.82	0.8	0.83
E_V (GPa)	101.46	103.49	112.44
E_R (GPa)	100.29	103.49	112.2
n_{max}	0.181	0.186	0.175
n_{min}	0.176	0.18	0.175
A	1.42	1.39	1.09
β (GPa)	0.0064	0.0058	0.0061

to the upper bound of G values) and G_R is Reuss's shear modulus (which is related to the lower bound of G values) and can be written as $G_V = \left(C_{11} - C_{12} + 3C_{44}\right)/5$ and $5/G_R = 4/\left(C_{11} - C_{12}\right) + 3/C_{44}$, respectively.

Table 3 shows calculated values of Voigt's isotropic shear modulus, Reuss's shear modulus, ratio of G/B, Young's modulus E, maximum and minimum Poisson's ration (n_{max}, n_{min}) and compressibility factor β for all the three crystals. It is seen that the isotropic shear modulus are such that the value of E_V and E_R increases from Ca_3PbO, Ca_3SnO and Ca_3GeO respectively. The ratio G/B is called Pugh's ratio which shows whether a material is brittle or ductile. For $G/B > 0.5$ shows brittle nature of the material but $G/B < 0.5$ shows that the material is ductile. For the three crystals, G/B values calculated are 0.82, 0.80 and 0.83 for Ca_3PbO, Ca_3SnO and Ca_3GeO respectively. This shows that these crystals are brittle. It can also be concluded that Ca_3GeO has the largest Young's modulus which is an indication that it is stiffer compared to the other two compounds.

For Poisson's ratio less than 0.25, the material shows strong covalent bonds and value larger than 0.25 indicates ionic bond [23] [24] [25] [26] [27]. As can be seen from our computations all our Poisson's ratios are less than 0.25 which is an indication that all these atoms have strong covalent bonds. For bulk materials, elastic anisotropy is determined by Zener anisotropy factor A which if is 1, shows that the material is isotropic otherwise the material is anisotropic. All three materials show factor of A as 1.42, 1.39 and 1.09 for Ca_3PbO, Ca_3SnO and

Ca_3GeO respectively. It can therefore be concluded that these compounds are anisotropic. This therefore implies that direction of pressure application is critical for maximum performance of these materials in thermoelectric design.

The compressibility is a measure of elasticity defined from the relation;

$$\beta = \frac{C_{11} - C_{12}}{\Omega} \tag{6}$$

$$\Omega = \left(C_{11} + C_{12}\right)C_{11} - 2C_{12}^2 \tag{7}$$

The compressibility values are found to be 0.0064 GPa^{-1}, 0.0058 GPa^{-1} and 0.0061 GPa^{-1} for Ca_3PbO, Ca_3SnO and Ca_3GeO respectively. Compressibility is the inverse of bulk modulus and therefore high value of β means low value of bulk modulus.

3.4. Dynamical Properties

Phonon dispersion relations are depicted in Figures 5-7 below. The vibration frequency is directly proportional to the energy.

The primitive cell of the atoms has five atoms which gives 15 phonon branches with 3 acoustic and 12 optical modes for all the crystals. In all the crystals, there is no gap between the acoustic and optical branches of these modes. The energy of dispersion is for Ca_3SnO is the least followed by Ca_3GeO and then Ca_3PbO. This is not proportional to atomic mass unit of the metal in the crystal. Figure 7 can be related to Figure 4 where there is lack of overlap between the conduction and valence band. This shows that tin will require more energy for the conduction electrons to fully participate in conduction compared to the other two crystals.

4. Conclusions

Study of antiperovskite Ca_3BO (B = Pb, Ge, Sn) using density functional theory

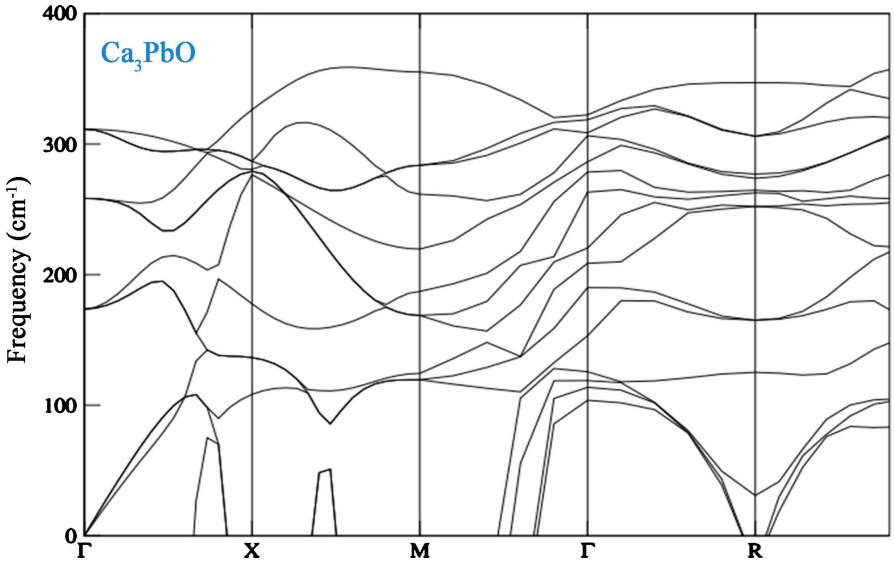

Figure 5. Dispersion relation of Ca_3PbO with the highest frequency at about 350 cm^{-1}.

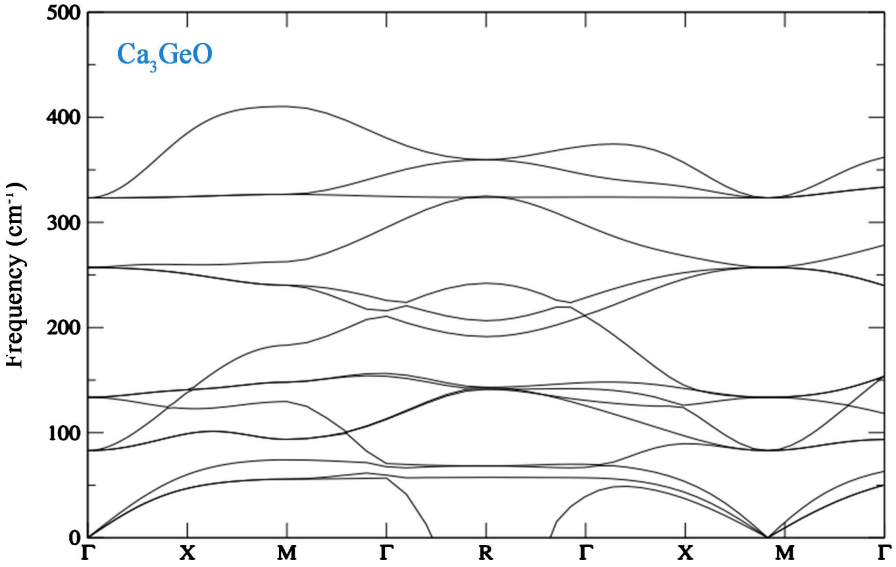

Figure 6. Dispersion relation of Ca_3GeO with highest frequency at about 400 cm^{-1}.

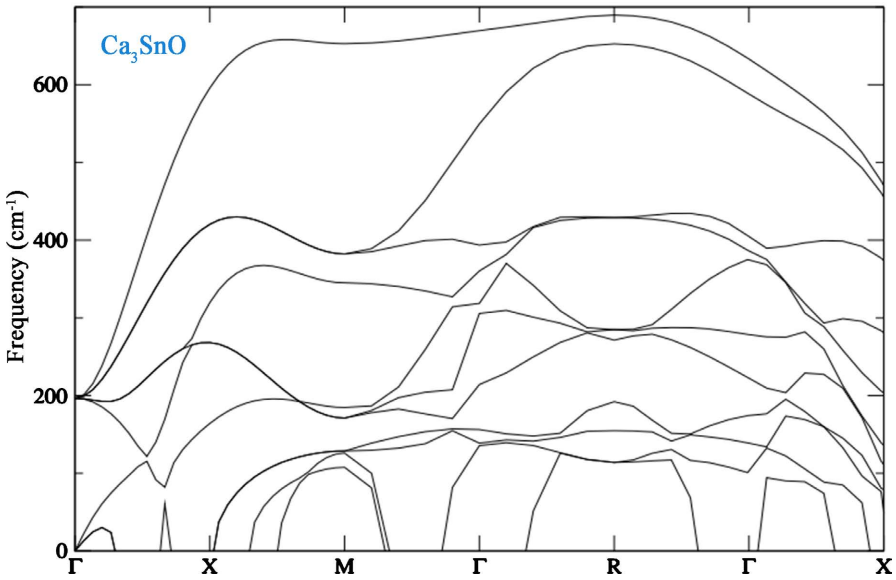

Figure 7. Dispersion relation of Ca_3SnO with the highest frequency at 620 cm^{-1}.

is here reported. The electronic structure studies show that these materials are conductors with similarities in properties as depicted by their band structures and projected density of states. There are also indicating stability from elastic constants study and derived properties. Phonon dispersion also points at the metallic nature of compounds CaBO. These crystals are therefore stable in their cubic states and are suitable for pressure-induced applications including thermoelectric applications

Acknowledgements

I acknowledge the support of computational resources provided by Centre for High Performance Computers, of Cape Town, South Africa.

Conflicts of Interest

The author declares no conflicts of interest regarding the publication of this paper.

References

[1] Kaur, T. and Sinha, M.M. (2021) Probing Thermoelectric Properties of High Potential Ca3PbO: An *Ab Initio* Study. *IOP Conference Series*: *Materials Science and Engineering*, **1033**, Article ID: 012080. https://doi.org/10.1088/1757-899X/1033/1/012080

[2] He, T., Huang, Q., Ramirez, A.P., *et al.* (2001) Superconductivity in the Non-Oxide Perovskite $MgCNi_3$. *Nature*, **411**, 54-56. https://www.nature.com/articles/35075014 https://doi.org/10.1038/35075014

[3] Henriques, J.M., *et al.* (2008) First-Principles Calculations of Structural, Electronic and Optical Properties of Orthorhombic $CaPbO_3$. *Journal of Physics D*: *Applied Physics*, **41**, 065405.

[4] Xu, G., Weng, H., Wang, Z., Dai, X. and Fang, Z. (2011) Chern Semimetal and the Quantized Anomalous Hall Effect in $HgCr_2Se_4$. *Physical Review Letters*, **107**, Article ID: 186806. https://doi.org/10.1103/PhysRevLett.107.186806

[5] Wang, Z., Weng, H., Wu, Q., Dai, X. and Fang, Z. (2013) Three-Dimensional Dirac Semimetal and Quantum Transport in Cd_3As_2. *Physical Review B*, **88**, Article ID: 125427. https://doi.org/10.1103/PhysRevB.88.125427

[6] Perdew, P., Ernzerhof, M. and Burke, K. (1996) Rationale for Mixing Exact Exchange with Density Functional Approximations. *The Journal of Chemical Physics*, **105**, 9982-9985. https://doi.org/10.1063/1.472933

[7] Giannozzi, P., *et al.* (2009) QUANTUM ESPRESSO: A Modular and Open-Source Software Project for Quantum Simulations of Materials. *Journal of Physics*: *Condensed Matter*, **21**, Article ID: 395502. https://doi.org/10.1088/0953-8984/21/39/395502

[8] Kohn, W. and Sham, L. (1965) Self-Consistent Equations Including Exchange and Correlation Effects. *Physical Review Journals Archive*, **140**, A1133-A1138. https://doi.org/10.1103/PhysRev.140.A1133

[9] Monkhorst, H.J. and Pack, J.D. (1976) Special Points for Brillouin-Zone Integrations. *Physical Review B*, **13**, 5188-5192. https://doi.org/10.1103/PhysRevB.13.5188

[10] Burkov, A.A., Hook, M.D. and Balents, L. (2011) Topological Nodal Semimetals. *Physical Review B*, **84**, Article ID: 235126. https://doi.org/10.1103/PhysRevB.84.235126

[11] Chung, D.Y., Hogan, T., Brazis, P., Rocci-Lane, M., Kannewurf, C., Bastea, M. and-Kanatzidis, M.G. (2000) CsBi4Te6: A High-Performance Thermoelectric Material for Low-Temperature Applications. *Science*, **287**, 1024-1027. https://doi.org/10.1126/science.287.5455.1024

[12] Obata, Y., Yukawa, R., Horiba, K., Kumigashira, H., Toda, Y., Matsuishi, S. and Hosono, H. (2017) ARPES Studies of the Inverse Perovskite Ca_3PbO: Experimental Confirmation of a Candidate 3D Dirac Fermion System. *Physical Review B*, **96**, Article ID: 155109. https://doi.org/10.1103/PhysRevB.96.155109

[13] Burganov, B., Adamo, C., Mulder, A., Uchida, M., King, P.D.C., Harter, J.W. and Shen, K.M. (2016) Strain Control of Fermiology and Many-Body Interactions in Two-Dimensional Ruthenates. *Physical Review Letters*, **116**, Article ID: 197003.

https://doi.org/10.1103/PhysRevLett.116.197003

[14] Kariyado, T. and Ogata, M. (2011) Three-Dimensional Dirac Electrons at the Fermi Energy in Cubic Inverse Perovskites: Ca_3PbO and Its Family. *Journal of the Physical Society of Japan*, **80**, Article ID: 083704. https://doi.org/10.1143/JPSJ.80.083704

[15] Murnaghan, F.D. (1994) The Compressibility of Media under Extreme Pressures. *Proceedings of the National Academy of Sciences of the United States of America*, **30**, 244-247. https://doi.org/10.1073/pnas.30.9.244

[16] Born, M. and Huang, K. (1956) Dynamical Theory of Crystal Lattices. Clarendon Press, Oxford.

[17] Mayer, B., Anton, H., Bott, E., *et al.* (2003) *Ab-initio* Calculation of the Elastic Constants and Thermal Expansion Coefficients of Laves Phases. *Intermetallics*, **11**, 23-32. https://doi.org/10.1016/S0966-9795(02)00127-9

[18] Widera, A. and Schäfer, H. (1980) Übergangsformen zwischen zintlphasen und echten salzen: Dieverbindungen A_3BO (MIT A = Ca Sr Ba und B = Sn Pb) Mater. *Materials Research Bulletin*, **15**, 1805-1809. https://doi.org/10.1016/0025-5408(80)90200-7

[19] Haddadi, K., Bouhemadou, A., Louail, L. and Bin, O.S. (2010) Inverse-Perovskite Oxides Ca_3 EO with E = Si, Ge, Sn, Pb: Structural, Elastic and Thermal Properties. *Solid State Communications*, **150**, 1995-2000. https://doi.org/10.1016/j.ssc.2010.08.021

[20] Nyawere, P.W.O., Makau, N.W. and Amolo, G.O. (2014) First-Principles Calculations of the Elastic Constants of the Cubic, Orthorhombic and Hexagonal Phases of BaF_2. *Physica B*: *Condensed Matter*, **434**, 122-128. https://doi.org/10.1016/j.physb.2013.10.051

[21] Mogulkoc, *et al.* (2018) Electronic Structure and Optical Properties of Novel Monolayer Gallium Nitride and Boron Phosphide Heterobilayers. *International Journal of Biosensors & Bioelectronics*, **4**, 70-75.

[22] Kaur, T. and Sinha, M.M. (2021) Probing Thermoelectric Properties of High Potential Ca_3PbO: An *Ab Initio* Study. *IOP Conference Series*: *Materials Science and Engineering*, **1033**, Article ID: 012080. https://doi.org/10.1088/1757-899X/1033/1/012080

[23] Rohr, C. (2010) Crystal Structure of Calcium Germanide Oxide, Ca_3GeO. *Zeitschrift für Kristallographie-Crystalline Materials*, **210**, 781.

[24] Batool, J., Alay-e-Abbas, S.M. and Amin, N. (2018) Thermodynamic, Electronic, and Magnetic Properties of Intrinsic Vacancy Defects in Antiperovskite Ca_3SnO. *Journal of Applied Physics*, **123**, Article ID: 161516. https://doi.org/10.1063/1.4994998

[25] Cherred, D., Maouche, M., Maanmache, M. and Krache, L. (2011) Influence of Valence Electron Concentration on Elastic, Electronic and Optical Properties of the Alkaline-Earth Tin Oxides A_3SnO (A=Ca, Sr and Ba): A Comparative Study with $ASnO_3$ Compounds. *Physica B*, **406**, 2714-2722.

[26] Wang, S.Q. and Ye, H.Q. (2003) *Ab Initio* Elastic Constants for the Lonsdaleite Phases of C, Si and Ge. *Journal of Physics*: *Condensed Matter*, **15**, Article 5307. https://doi.org/10.1088/0953-8984/15/30/312

[27] Rajeswarapalanichamiy, R., Priyanga, G.S., Cinthia, A.J. and Iyakutti, K. (2015) Structural stability, electronic structure and mechanical properties of ZnN and CdN: A first principles study. *Computational Materials Science*, **99**, 117-124. https://doi.org/10.1016/j.commatsci.2014.12.012